Carbon counter electrode mesoscopic ambient processed & characterised perovskite for adaptive BIPV fenestration

Aritra Ghosh[*], Shubhranshu Bhandari, Senthilarasu Sundaram, Tapas K. Mallick

Environment and Sustainability Institute (ESI), University of Exeter, Penryn Campus, TR10 9FE, United Kingdom

ABSTRACT

In this work, carbon counter electrode perovskite was developed at the laboratory environment and building integrated photovoltaic (BIPV) window application using this material was investigated. At 1 sun (1000 W/m2) continuous incident solar radiation from an indoor simulator, this particular type of perovskite had 8.13% efficiency. Average solar and visible transmittance of this perovskite BIPV window was 30% and 20% respectively. Solar heat gain for different incident angle was evaluated for this perovskite glazing. For the University of Exeter, Penryn (50.16° N, 5.10° W) UK location, solar heat gain coefficient (SHGC) or solar factor (SF) varied from 0.14 to 0.33 at the highest and lowest incident angle respectively. Overall heat transfer coefficient (U-value) of 5.6 W/m²K was realized for this glazing while calculation was performed by window performance analysis programme, WINDOW 6.0. Daylight glare control potential of this glazing was investigated using subjective rating methods and comfortable daylight penetrated through glazing in a typical cloudy condition. Colour properties of this material showed that 20% visible transmittance is threshold limit, and below this value colour or visual comfort using this glazing is not achievable.

1. Introduction

The building sector accounts for 40% of total energy consumption while emits one-third of the world's global greenhouse gases. Reduction of building energy consumption is essential to limit the global average temperature increment to well below 2 °C above pre-industrial levels as committed in December 2015, Paris agreement [1]. Traditional transparent single- and double-glazed windows enhance the building energy consumption being the weakest part of a building envelope whilst it brings external sunlight and fresh air into the indoor space. Thus, to maintain view and energy loss reduction using a single unit window, semi-transparent and highly insulating are the precondition. Inclusion of photovoltaic (PV) device in a building can replace the low energy performing window [2].

Integration of PV devices into a building includes building attached/applied PV (BAPV) and building integrated PV (BIPV). BAPV types are the addition of a PV technology into a building, which does not disturb the existing building structure [3] and has no impact on building heat loss or heat gain. BIPV systems are an integral part of a building which replaces the traditional building envelope (e.g. wall, roof, and window). BIPVs are often semi-transparent in nature and has an impact on controlling of building heating and cooling load. Recent trends of buildings are large glazed façade types where BIPV window products are getting higher priority. Semi-transparent or transparent type BIPV windows are aesthetic in nature, allow daylight, control solar heat gain, and generates electricity [4].

For BIPV window, types of different PV includes crystalline silicon [5], amorphous silicon, cadmium telluride [6,7], CIGS, dye-sensitized solar cell (DSSC) [8], perovskite [9]. Among all the different types of PV, crystalline silicon is the mature, highly durable and highly efficient [10]. Its opaque in nature can be overcome by maintaining space between two cells [11]. Vacuum integrated BIPV window is also reported which reduces the overall heat loss [5]. However, at suboptimal tilt angle or at high temperature, c-Si PV outperforms [12,13].

For building's façade or window application, semitransparency is a precondition. Semitransparency due to tunable bandgap PV technologies has the potential to match the thermo-optical requirement for architectural application. Thin film technologies and DSSC and perovskite material possess semi-transparent nature,
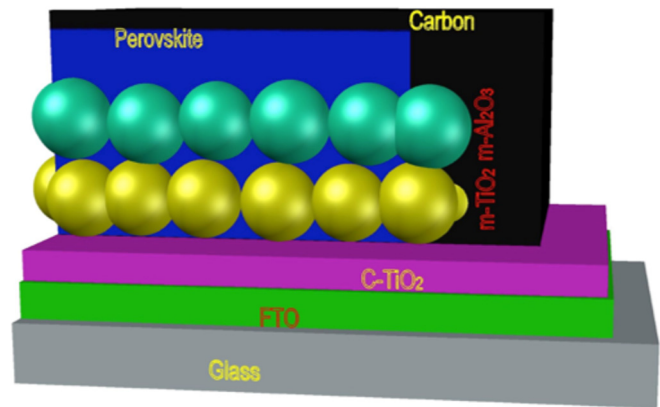
Fig. 1. Schematic of carbon counter electrode perovskite.

characterised carbon counter electrode perovskite was investigated for fenestration application. From measured transmittance data, solar factor, angular transmittance and angular solar factor have also been calculated to understand the suitability of this material for building's fenestration application. Daylight glare and quality of light at indoor space for this glazing were also evaluated.

2. Experiment

2.1. Glazing fabrication

Fabricated perovskite glazing had FTO/c-TiO$_2$/mp-TiO$_2$/Li-TFSI/Al$_2$O$_3$/C structure. Carbon paste was prepared as follows: 1 g of graphite powder (Sigma−Aldrich) was mixed with 0.2 g of carbon black powder (Alfa Aesar) in 3.5 mL of terpineol (Sigma−Aldrich). Then, 0.1 g of ZrO$_2$ powder (Sigma−Aldrich) and 1.5 g of ethyl cellulose (15 wt % in ethanol) (Sigma−Aldrich) were added, followed by ball milling overnight. The additive was added before ball milling by 0.4 mL of WO$_3$ nanoparticle ink (2.5 wt % in isopropanol, Sigma−Aldrich, 793353).

The perovskite precursor solution was prepared as follows: 0.198 g CH$_3$NH$_3$I (MAI) (Sigma−Aldrich) and 0.573 g PbI$_2$ (Sigma−Aldrich) were dissolved in 1 ml γ-butyrolactone (Sigma−Aldrich) and then stirred at 60 °C for overnight.

The fabrication of perovskite based mesoscopic solar cells: Fluorine-doped tin oxide (FTO) coated glass was first etched with HCl solution and zinc powder and then cleaned sequentially with detergent, deionized water, acetone, ethanol and deionized water. TiO$_2$ compact layer was spin coated onto cleaned FTO transparent glass substrates by using 0.15 M titanium dissopropoxidebis-(acetylacetonate) (Tiacac) (75 wt% in isopropanol, Sigma−Aldrich) in a 2-propanol (99.9%, Sigma−Aldrich) solution at 2000 rpm for 30 s, followed by drying at 115 °C for 5 min and cooled down to room temperature. Further coating (1000 rpm, 30 s) from 0.3 M Tiacac solution was carried out and dried at 115 °C for 5 min. The dried TiOx coated samples were heated at 415 ± 10 °C for 30 min in a hot plate. The mesoporous TiO$_2$ layer was prepared with diluted TiO$_2$ paste (18NRT from Dyesol Company; w/w = 1:3.5 in ethanol) by spin coating at 2000 rpm for 30 s and heated at 500 °C for 60 min. Further, the mesoporous TiO$_2$ layer was doped with lithium via spin coating (1000 rpm, 15 s) of 0.1 M lithium bis(trifluoromethanesulfonyl)imide (Li-TFSI) solution in acetonitrile and annealed at 415 ± 15 °C for 30 min. Then, the Al$_2$O$_3$ mesoporous layer was followed by spin coating with diluted Al$_2$O$_3$ paste (Sigma Aldrich, 702129; v/v = 1:2 in isopropanol) at 2000 rpm for 30s and heated at 150 °C for 30 min. The mesoscopic carbon layer was

thus suitable for non-opaque building envelope application. Organic-inorganic hybrid perovskite solar cell has achieved power conversion efficiency up to 22% which rendered them as the most promising PV technology. However, this success has been hindered due to poor stability of this perovskite PV cell under ambient condition [14]. Fabrication of this type of PV mostly restricted to control environment glove box fabrication process to avoid the humidity. Thus, environmentally benign perovskites are the critical, yet challenging aspects for perovskite BPV window research. Presently ambient processed perovskite has also been investigated to protect the perovskite absorber layer from exposure to moisture, oxygen, and UV light [15,16].

Use of mesoscopic structure to prepare perovskite PV, avoids the requirement of costly hole-transporting materials (HTMs). Thus overall perovskite synthesis process becomes cost-effective and simpler [17]. However, this structure is still expensive due to the use of costly metal such as gold (Au), silver (Ag) for the counter electrode, which is an impediment for large scale production. Carbon is an alternative abundantly available low-cost material, which can be used for the counter electrode (CE) [18]. The work function of carbon (5.0 eV) is close to gold (Au) (5.1 eV) [19]. Hole-conductor-free CH$_3$NH$_3$PbI$_3$ perovskite/TiO$_2$ heterojunction solar cells showed 6.64% power conversion efficiency using carbon CE [20]. Fig. 1 shows the schematic of a typical carbon counter electrode perovskite PV cell.

BIPV window application and energetic analysis based on perovskite PV is limited work compared to the exploration of different new perovskite device fabrication methods. For window application, 30% transparent neutral colour perovskite PV was fabricated which was 3.5% efficient to convert solar energy to electrical power [21]. In another work, transparency and power conversion efficiency of neutral colored solid-state planar heterojunction perovskite PV cells were employed in simulation work to find out its visual comfort and energy performance potential [22]. Potential of perovskite BIPV window for Italian climate was investigated which showed 18% yearly building energy saving compared to clear single pane window [9].

In this work, for the first-time ambient processed and

finally screen-printed with the as-prepared carbon paste and sintered at 450 °C for 30 min. After cooling down to room temperature, the perovskite precursor solution with an appropriate amount was infiltrated by drop casting via the top of the carbon counter electrode. After infiltrating the active area of the device, the device was spin-coated at 1000 rpm for 15s. Finally, after drying at 50 °C for 1 h, the mesoscopic solar cells containing perovskite were obtained as shown in Fig. 2.

2.2. Optical and electrical performance

Spectral characterisation for fabricated perovskite was performed using an ultra-violet–visible–near infrared (UV/VIS/NIR) spectrophotometer (PerkinElmer® Lambda 1050) equipped with an integrating sphere (150 mm diameter) with 10 nm interval as shown in Fig. 3 and described in Ref. [23].

Electrical performance of this carbon counter electrode mesoscopic ambient processed perovskite PV was characterised at 0° from horizontal under the Wacom Super Solar Simulators for providing highly collimated illumination as shown in Fig. 4. The J–V characteristic evaluation of this PV cell was recorded using EKOMP-160i I – V Tracer. Kipp and Zonen pyranometer measured the intensity and data were recorded by using the data logger and collected from a computer.

3. Methodology

3.1. Calculation of glazing transmission and reflection

Luminous transmission or reflection can be obtained from equations (1) and (2) [23].

Luminous transmission or reflection $L_v(\alpha)$

$$= \frac{\sum_{\lambda=380nm}^{780nm} D_{65}(\lambda)K(\lambda,\alpha)V(\lambda)\Delta\lambda}{\sum_{\lambda=380nm}^{780nm} D_{65}(\lambda)V(\lambda)\Delta\lambda} \quad (1)$$

For transmission $L_v = \tau_v$ and $K(\lambda,\alpha) = T(\lambda,\alpha)$; for reflection $L_v = \rho_v$ and $K(\lambda,\alpha) = R(\lambda,\alpha)$
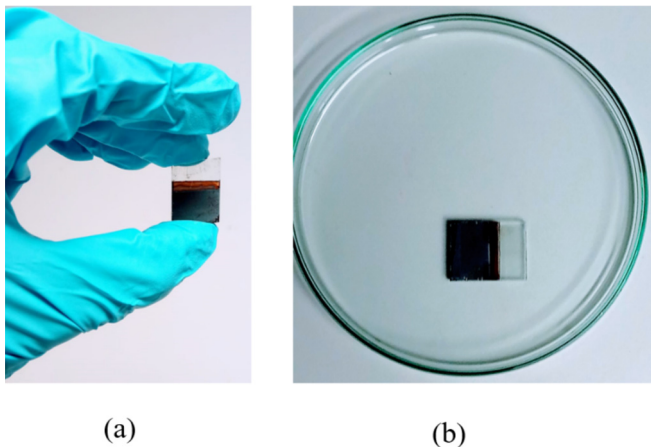

(a) (b)

Fig. 2. Fabricated carbon counter electrode Perovskite.

$$\text{Solar transmission } \tau_s(\alpha) = \frac{\sum_{\lambda=300nm}^{2500nm} S(\lambda)T(\lambda,\alpha)\Delta\lambda}{\sum_{\lambda=300nm}^{2500nm} S(\lambda)\Delta\lambda} \quad (2)$$

3.2. Solar heat gain due to angular transmission

Solar heat gain coefficient (SHGC) or solar factor (SF) [24] is an indispensable parameter for a window as it determines the amount of transmitted solar energy (SE) through the window and absorbed SE by the window and reemitted inwards [25]. SHGC at oblique angles is the outmost important parameters for yearly and daily building energy consumption calculation. SHGC at an oblique incident angle is given by equation (3). Solar heat gain depends on the transmittance of the glazing which is achieved by using equation (4) [26–28].

$$g(\theta) = \tau_s(\theta) + [1 - \tau_s(\theta) - \rho_s(\theta)]\frac{h_i}{h_i + h_e} \quad (3)$$

$$\tau_s(\theta) = \frac{1}{2}\left[\frac{1 - \left\{\frac{\sin(\theta-n)}{\sin(\theta+n)}\right\}^2}{1 + (2n_g - 1)\left\{\frac{\sin(\theta-n)}{\sin(\theta+n)}\right\}} + \frac{1 - \left\{\frac{\tan(\theta-n)}{\tan(\theta+n)}\right\}^2}{1 + (2n_g - 1)\left[\frac{\tan(\theta-n)}{\tan(\theta+n)}\right]^2}\right]$$
$$\times \exp\left(\frac{-k_g N_g t_g}{\cos\theta}\right)$$

(4)

Where extinction coefficient (k) and refractive index (n) are given by equations (5) and (6)

$$k = -\frac{\lambda}{4\pi d}\ln t \quad (5)$$

$$n = \frac{(1+\sqrt{r})}{(1-\sqrt{r})} \quad (6)$$

$$r = \frac{\beta - \sqrt{\beta^2 - 4(2-\rho)\rho}}{2(2-\rho)}; t = \frac{(\rho-r)}{r\tau} \beta = \tau^2 - \rho^2 + 2\rho + 1$$

3.3. Daylight glare analysis

Daylight glare evaluation for perovskite based BIPV glazing is essential to understand the building occupants' comfort. Thus, theoretically glare control potential using this glazing was identified from measured outdoor illuminance on a vertical plane as shown in Fig. 5. The glare subjective rating (SR) is [29] shown in equation (7) which was employed in this work. This SR index allows discomfort glare estimation experienced by subjects when working at a visual daylight task (VDT) placed against a window of high or non-uniform luminance.

$$SR = 0.1909E_v^{0.31} \quad (7)$$

The reason for selecting this index is the engagement of only one photosensor which can save time and cost. SR for typical sunny day, intermittent and overcast cloudy day in Penryn UK (50.16° N, 5.10° W) was investigated. Perovskite glazing was considered vertically placed, south facing, having a dimension of $30 \times 30 \times 0.5$ ($l \times w \times h$) cm in the scale model. This large area resembles perovskite as large façade while the internal surface was painted in white colour with a reflectance of 0.8 [30]. Internal vertical
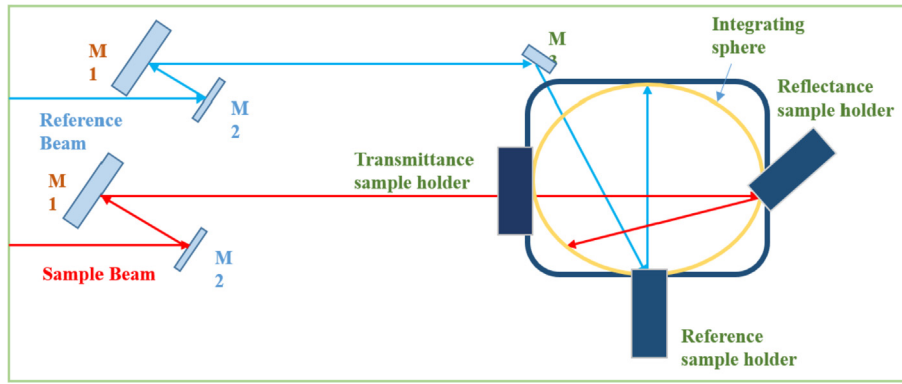
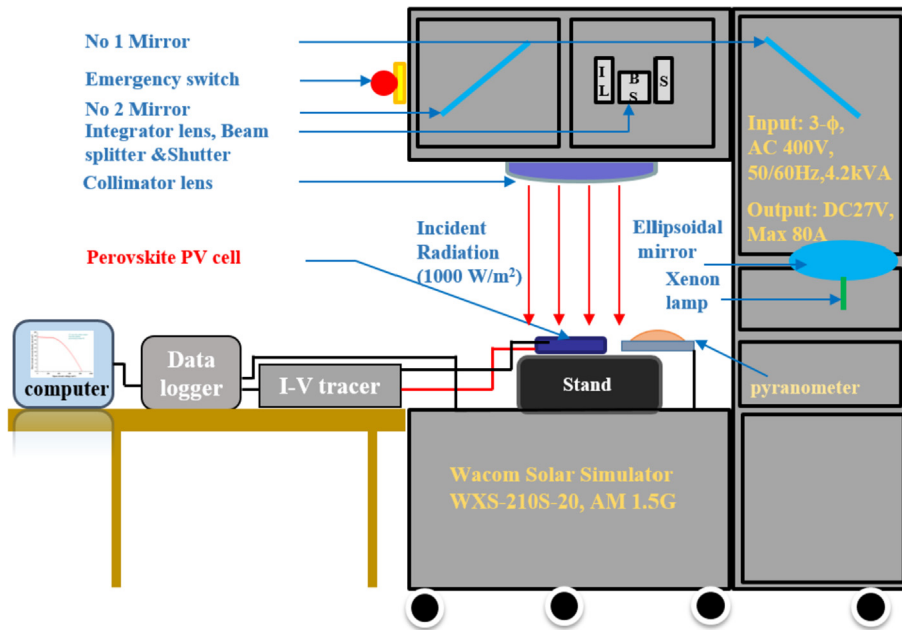**Fig. 3.** Schematic representation of the UV/vis/NIR spectrophotometer used for spectral measurements.

Fig. 4. Schematic of indoor electrical characterisation set up using AAA standard simulator.
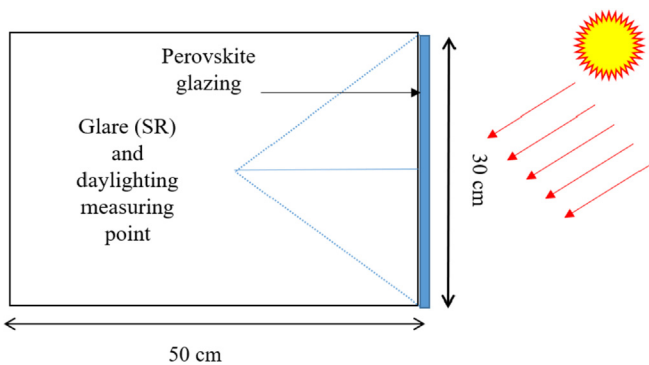

Fig. 5. Schematic cross section of a room with perovskite glazing mounted on vertical south façade.

illuminance (E_V) facing the window (worst case) was measured at the centre of the room. The criterion scale of discomfort glare subjective rating is given in Table 1. This method also allows the non-intrusive measuring equipment necessary for scale model daylighting assessments [31,32].

Table 1
Criterion scale of discomfort glare subjective rating (SR) [29].

Comfort level indicator	Glare subjective rating (SR)
Just intolerable	2.5
Just disturbing	1.5
Just noticeable/accepting	0.5

3.4. Colour properties

Quality and quantity of entering daylight are characterised by correlated colour temperature (CCT) and colour rendering index (CRI). Perfect transmitted daylight should have CCT from 3000 K to 7500 K while CRI close to 100 is required. CRI below 80 is not suitable for glazing application.

CCT was calculated from McCamy's equation (8) [33].

$$CCT = 449n^3 + 3525n^2 + 6823.3n + 5520.33 \qquad (8)$$

where

$$n = \frac{(x - 0.3320)}{(0.1858 - y)}$$

$$x = \frac{X}{X + Y + Z}, \; y = \frac{Y}{X + Y + Z}$$

$$X = \sum_{380nm}^{780nm} D_{65}(\lambda) \, \tau(\lambda) \overline{x}(\lambda) \, \Delta\lambda \tag{9}$$

$$Y = \sum_{380nm}^{780nm} D_{65}(\lambda) \, \tau(\lambda) \overline{y}(\lambda) \, \Delta\lambda \tag{10}$$

$$Z = \sum_{380nm}^{780nm} D_{65}(\lambda) \, \tau(\lambda) \overline{z}(\lambda) \, \Delta\lambda \tag{11}$$

X, Y and Z are the tristimulus values which represent the three-colour perception values of the human eye response, Luminous transmittance values τ_v, $D_{65}(\lambda)$ is the spectral power distribution of CIE standard illuminant D_{65}, $V(\lambda)$ is the photopic luminous efficiency function of the human eye and $\Delta\lambda = 10$ nm.

3.5. CRI is given by

$$CRI = \frac{1}{8}\sum_{i=1}^{8}\left[100 - 4.6\left\{\sqrt{\left(U_{t,i}^{*}-U_{r,i}^{*}\right)^2 + \left(V_{t,i}^{*}-V_{r,i}^{*}\right)^2 + \left(W_{t,i}^{*}-W_{r,i}^{*}\right)^2}\right\}\right] \tag{12}$$

Conversion into the CIE 1964 uniform colour space system for each test colours the conversion is performed using colour space system $W_{t,i}^{*}$, $U_{t,i}^{*}$, $V_{t,i}^{*}$ whereas $W_{r,i}^{*}$, $U_{r,i}^{*}$, $V_{r,i}^{*}$ represents for each test colours, lighted by the standard illuminant D_{65} without the glazing

$$W_{t,i}^{*} = 25\left(\frac{100Y_{t,i}}{Y_t}\right)^{1/3} - 17 \tag{13}$$

$$U_{t,i}^{*} = 13W_{t,i}^{*}\left(u_{t,i}^{'} - 0.1978\right) \tag{14}$$

$$V_{t,i}^{*} = 13W_{t,i}^{*}\left(V_{t,i}^{'} - 0.3122\right) \tag{15}$$

4. Results and discussion

Measured J–V curves of the carbon-electrode mesoscopic ambient processed perovskite PV cell, is shown in Fig. 6. Experiment was performed under simulated AM 1.5 solar irradiation at an intensity of 100 mWcm−2 measured at room temperature. This cell exhibited a short-circuit current density (J_{SC}) of 18.3 mA/cm^2, open-circuit voltage (V_{OC}) of 790 mV, Fill factor (FF) of 56%, and showed the device efficiency of 8.13% and the output power per unit weight of 14.4 mW/g.

Fig. 7 shows the transmittance of the newly developed perovskite glazing. For comparison, the product of relative spectral
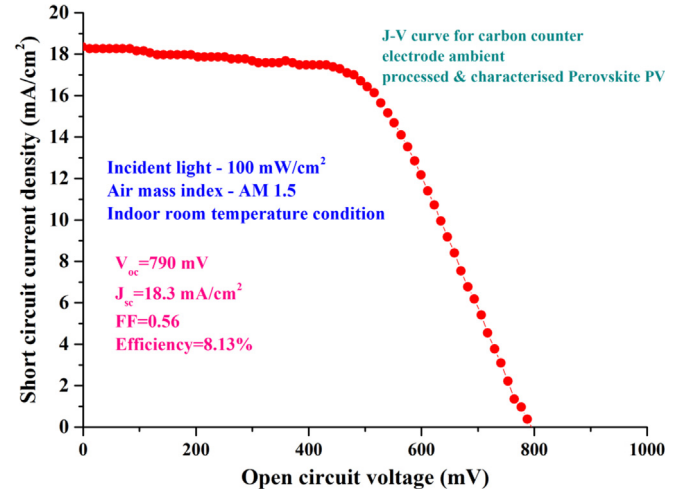

Fig. 6. The J–V curves of the carbon-electrode mesoscopic ambient processed perovskite PV cell.

distribution of illuminant D65 (Dλ) and the spectral luminous efficiency for photopic vision V(λ) has also been added which ranges from 400 to 700 nm with its peak at 555 nm. Bandwidth under 380−780 nm performance of the perovskite glazing is lower than the bandwidth between 780 nm and 2500 nm. Average solar transmittance was 30% whilst visible transmittance was 20%.

Fig. 8 and Fig. 9 show the angular behaviour of carbon counter electrode perovskite glazing's transmittance and the solar factor which were calculated using equations (11) and (12) respectively for the University of Exeter, Penryn (50.16° N, 5.10° W) UK location. For this particular location, the incident angle between impinging solar radiation and vertical plane glazing varies from 13⁰ to 87⁰ throughout the year. Using angular transmission equation, high transmission of 30% for vertical facades made by this perovskite glazing is possible whereas, low transmission value of 10% is achievable at a higher incident angle. SF is directly related to glazing transmission, thus its behaviour changed similar to glazing transmission. Maximum and minimum SFs were possible to 0.33 and 0.14 respectively from this glazing.

Due to the smaller device size, overall heat transfer coefficient (*U*-value) was evaluated by using WINDOW software from LBNL. This perovskite glazing was fabricated by sandwiching between two glass, each was 3 mm thick while visible and solar
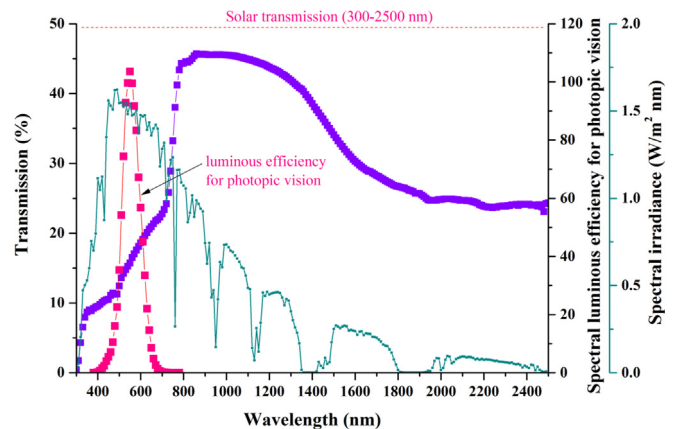

Fig. 7. Optical transmittance of semi-transparent perovskite PV for adaptive window application.
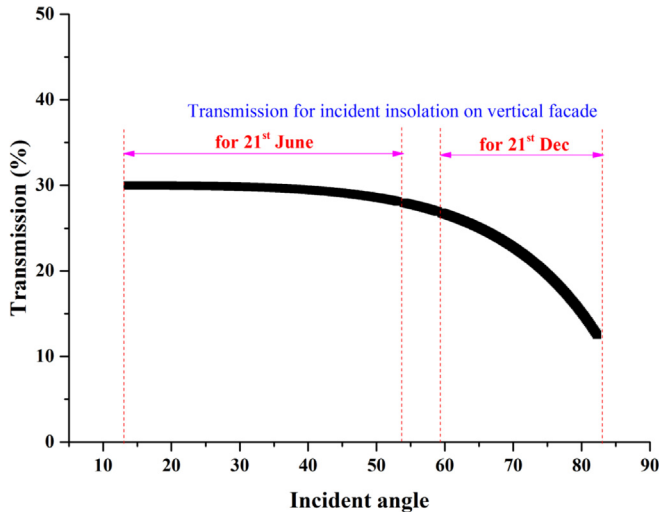
Fig. 8. Angular transmission of carbon counter electrode perovskite glazing for varying incident angle.
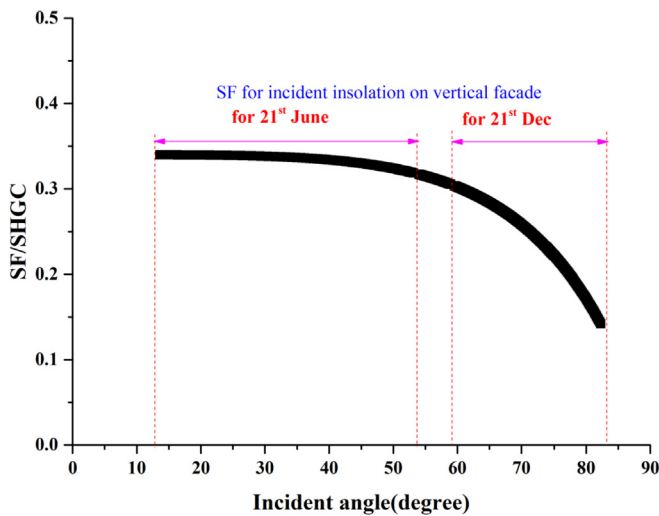

Fig. 9. Angular solar factor of carbon counter electrode perovskite glazing for varying incident angle.

transmittances were 90% and 83% respectively. The environmental condition was considered National Fenestration Rating Council (NFRC) standard where the wind speed was 5.5 m/s, the indoor air temperature was 21 °C and the outdoor air temperature was −18 °C. U-value of this glazing without frame was 5.61 W/m^{2}K. As this device was fully sandwiched and no air gap or any other space was provided between two glass panes, high U-value was achieved. This result was very similar to suspended particle device glazing which showed 5.9 W/m^{2}K U-value when the experiment was performed at an outdoor condition in a temperate climate using test cell [34]. To observe variation in result, 2 mm space filled with different inert gasses were provided between two sheets of glass. Presence of Argon, U -value was 3.4 W/m^{2}K, while krypton and Xenon gave 2.8 W/m^{2}K and 2.67 W/m^{2}K respectively. Presence of air gave U-value of 3.8 W/m^{2}K which was maximum compared to other inert gasses.

Lower solar gain and higher U-value makes this glazing a suitable candidate for warmer climate and summer season when indoor room temperature needs to be low to trim down air conditioning load and enhance occupant's thermal comfort.

Ambient daylight in an indoor space improves people's cognitive work, psychological health and their productivity. Fig. 10 shows the glare and daylighting control potential of this perovskite glazing for façade application. Internal illuminance pattern changed in a similar way to external illuminance. Internal illuminance level was compared with useful daylight illuminance (UDI) index which indicates illuminance level between 100 and 2000 lux is allowable for indoor [35]. Clear sunny day UDI was allowable till 9:00 a.m. whereas for an overcast day and intermittent day UDI was maintained by offering comfort level. Glare level crossed in higher order from its standard level for a clear sunny day. SR index showed that the glare level crossed the disturbing level (SR = 1.5) for the clear sunny day while maintaining the limit for an intermittent and overcast day. It is evident that 20% visible transparent perovskite showed allowable glare level for an intermittent and overcast cloudy day while was crossed the limit at the mid-day period for a clear sunny day.

Colour properties of perovskite glazing were calculated using equation (8) (CCT) and 12 (CRI). CRI for this particular glazing material was 80 while CCT was 4457.57 K. This values just satisfy the acceptance level for the comfort level criteria as prescribed in CIE CIR [36,37] and IES TM 30—15 [38]. For colour comfort, CRI should be above 80 and CCT should be between 3000 K and 7500 K.
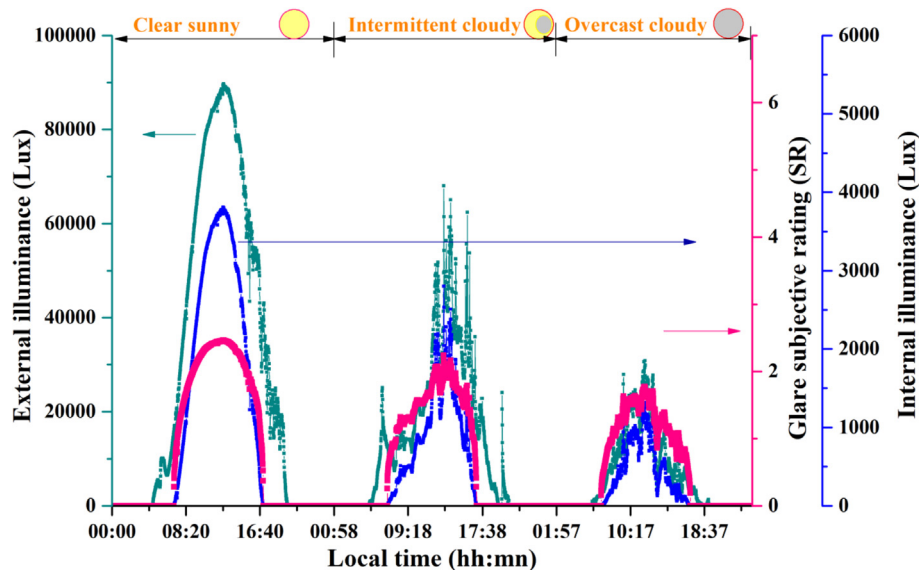

Fig. 10. Glare and daylight for Perovskite glazing.

However, glazings having lower transmittance always offer below 80 CRI. Glazing transmittance below 5% [39] for switchable suspended particle device glazing showed CRI of 60, while in another work, 5% transparent electrochromic showed CRI of 65 [40]. For solar and daylighting control glazing, the lower transmission is required but lower transmittance also promotes lower colour comfort. Thus solar-daylighting control and colour comfort both in the same system is hard to achieve. It is also confirmed that optimizing thermal and visual comfort is a difficult task due to the diurnal movement of the sun which gives different incident solar radiation including daylight for different hours.

5. Conclusions

In this work for the first-time carbon counter electrode-based perovskite was fabricated to investigate its potential for BIPV window application. The electrical performance was investigated at indoor climatic condition under 1 sun exposure from a continuous AAA standard simulator. The efficiency of this device was 8.13%, while current density was 18.3 mA/cm^2. Thermal and daylighting performance of this perovskite device was investigated for thermal and visual comfort analysis. Fabricated glazing showed 20% visible transmission while the average solar transmission was 30%. Visible transmission of glazing changed from 10 to 30% while the incident angle changed from 90° to 10° respectively. This perovskite glazing's solar factor varied between 0.14 and 0.33 for highest and lowest incident angle respectively at Penryn, UK location. Overall heat transfer coefficient was calculated using WINDOW software from LBNL. High *U*-value of 5.61 W/m^{2}K was achieved while the wind speed was 5.5. m/s and the indoor and outdoor air temperature was 21 °C, and −18 °C respectively. Daylight control potential of this glazing was investigated using subjective glare rating method. Higher glare amount was obtained at mid-day period for a clear sunny day. To achieve the further low value of daylight or glare, transmission reduction is essential however lower transmission will reduce the quality of light.

Acknowledgement

References

[1] A. Bauer, K. Menrad, Standing up for the Paris Agreement : Do global climate targets influence individuals ' greenhouse gas emissions ? Environ. Sci. Policy 99 (2019) 72—79, https://doi.org/10.1016/j.envsci.2019.05.015.

[2] A. Ghosh, B. Norton, Advances in switchable and highly insulating autonomous (self-powered) glazing systems for adaptive low energy buildings, Renew. Energy 126 (2018) 1003—1031, https://doi.org/10.1016/j.renene.2018.04.038.

[3] C. Peng, Y. Huang, Z. Wu, Building-integrated photovoltaics (BIPV) in architectural design in China, Energy Build. 43 (2011) 3592—3598, https://doi.org/10.1016/j.enbuild.2011.09.032.

[4] M. Saifullah, J. Gwak, J.H. Yun, Comprehensive review on material requirements, present status, and future prospects for building-integrated semitransparent photovoltaics (BISTPV), J. Mater. Chem. A. 4 (2016) 8512—8540, https://doi.org/10.1039/C6TA01016D.

[5] A. Ghosh, S. Sundaram, T.K. Mallick, Investigation of thermal and electrical performances of a combined semi- transparent PV-vacuum glazing, Appl. Energy 228 (2018) 1591—1600, https://doi.org/10.1016/j.apenergy.2018.07.040.

[6] H. Alrashidi, A. Ghosh, W. Issa, N. Sellami, T.K. Mallick, S. Sundaram, Evaluation of solar factor using spectral analysis for CdTe photovoltaic glazing, Mater. Lett. 237 (2019) 332—335, https://doi.org/10.1016/j.matlet.2018.11.128.

[7] Y. Sun, K. Shanks, H. Baig, W. Zhang, X. Hao, Y. Li, B. He, R. Wilson, H. Liu, S. Sundaram, J. Zhang, L. Xie, T. Mallick, Y. Wu, Integrated CdTe PV glazing into windows: energy and daylight performance for different architecture designs, Appl. Energy 231 (2018) 972—984, https://doi.org/10.1016/j.apenergy.2018.09.133.

[8] A. Ghosh, P. Selvaraj, S. Sundaram, T.K. Mallick, The colour rendering index and correlated colour temperature of dye-sensitized solar cell for adaptive glazing application, Sol. Energy 163 (2018) 537—544, https://doi.org/10.1016/j.solener.2018.02.021.

[9] A. Cannavale, L. Ierardi, M. Hörantner, G.E. Eperon, H.J. Snaith, U. Ayr, F. Martellotta, Improving energy and visual performance in offices using building integrated perovskite-based solar cells: a case study in Southern Italy, Appl. Energy 205 (2017) 834—846, https://doi.org/10.1016/j.apenergy.2017.08.112.

[10] M.A. Green, K. Emery, Y. Hishikawa, W. Warta, E.D. Dunlop, Solar cell efficiency tables (Version 45), Prog. Photovolt. Res. Appl. 23 (2015) 1—9, https://doi.org/10.1002/pip.

[11] A. Ghosh, S. Sundaram, T.K. Mallick, Colour properties and glazing factors evaluation of multicrystalline based semi-transparent Photovoltaic-vacuum glazing for BIPV application, Renew. Energy 131 (2019) 730—736, https://doi.org/10.1016/j.renene.2018.07.088.

[12] M.A. Green, General temperature dependence of solar cell performance and implications for device modelling, Prog. Photovolt. Res. Appl. 11 (2003) 333—340, https://doi.org/10.1002/pip.496.

[13] O. Dupré, R. Vaillon, M.A. Green, Physics of the temperature coefficients of solar cells, Sol. Energy Mater. Sol. Cells 140 (2015) 92—100, https://doi.org/10.1016/j.solmat.2015.03.025.

[14] M. Grätzel, The light and shade of perovskite solar cells, Nat. Mater. 13 (2014) 838—842, https://doi.org/10.1038/nmat4065.

[15] A. Roy, P. Selvaraj, P. Sujatha Devi, S. Sundaram, Morphology tuned BaSnO3active layer for ambient perovskite solar cells, Mater. Lett. 219 (2018) 166—169, https://doi.org/10.1016/j.matlet.2018.02.055.

[16] Q. Tai, P. You, H. Sang, Z. Liu, C. Hu, H.L.W. Chan, F. Yan, Ambient air irrespective of the humidity, Nat. Commun. 6 (2016) 1—8, https://doi.org/10.1038/ncomms11105.

[17] L. Etgar, P. Gao, Z. Xue, Q. Peng, A.K. Chandiran, B. Liu, Mesoscopic CH 3 NH 3 PbI 3/TiO 2 Heterojunction Solar Cells, 2012, pp. 8—11, https://doi.org/10.1021/ja307789s.

[18] L. Liu, A. Mei, T. Liu, P. Jiang, Y. Sheng, L. Zhang, H. Han, Fully printable mesoscopic perovskite solar cells with organic silane self-assembled monolayer, J. Am. Chem. Soc. 137 (2015) 1790—1793, https://doi.org/10.1021/ja5125594.

[19] Z. Ku, Y. Rong, M. Xu, T. Liu, H. Han, Full printable processed mesoscopic CH3 NH3 PbI 3/TiO2 heterojunction solar cells with carbon counter electrode, Sci. Rep. 3 (2013), https://doi.org/10.1038/srep03132.

[20] Z. Ku, Y. Rong, M. Xu, T. Liu, H. Han, Full Printable Processed Mesoscopic, 2013, https://doi.org/10.1038/srep03132.

[21] G.E. Eperon, V.M. Burlakov, A. Goriely, H.J. Snaith, Neutral color semitransparent microstructured perovskite solar cells, ACS Nano 8 (2014) 591—598, https://doi.org/10.1021/nn4052309.

[22] A. Cannavale, M.H.?? rantner, G.E. Eperon, H.J. Snaith, F. Fiorito, U. Ayr, F. Martellotta, Building integration of semitransparent perovskite-based solar cells: energy performance and visual comfort assessment, Appl. Energy 194 (2017) 94—107, https://doi.org/10.1016/j.apenergy.2017.03.011.

[23] A. Ghosh, T.K. Mallick, Evaluation of optical properties and protection factors of a PDLC switchable glazing for low energy building integration, Sol. Energy Mater. Sol. Cells (2017), https://doi.org/10.1016/j.solmat.2017.10.026, 0—1.

[24] T.E. Kuhn, Calorimetric determination of the solar heat gain coefficient g with steady-state laboratory measurements, Energy Build. 84 (2014) 388—402, https://doi.org/10.1016/j.enbuild.2014.08.021.

[25] M.C. Singh, S.N. Garg, An empirical model for angle-dependent g-values of glazings, Energy Build. 42 (2010) 375—379, https://doi.org/10.1016/j.enbuild.2009.10.004.

[26] A. Ghosh, B. Norton, A. Duffy, Behaviour of a SPD switchable glazing in an outdoor test cell with heat removal under varying weather conditions, Appl. Energy 180 (2016) 695—706, https://doi.org/10.1016/j.apenergy.2016.08.029.

[27] A. Ghosh, B. Norton, A. Duffy, Effect of sky conditions on light transmission through a suspended particle device switchable glazing, Sol. Energy Mater. Sol. Cells 160 (2017) 134—140, https://doi.org/10.1016/j.solmat.2016.09.049.

[28] A. Ghosh, B. Norton, A. Duffy, Measured thermal & daylight performance of an evacuated glazing using an outdoor test cell, Appl. Energy 177 (2016) 196—203, https://doi.org/10.1016/j.apenergy.2016.05.118.

[29] E.S. Lee, D.L. DiBartolomeo, Application issues for large-area electrochromic windows in commercial buildings, Sol. Energy Mater. Sol. Cells 71 (2002) 465—491, https://doi.org/10.1016/S0927-0248(01)00101-5.

[30] A. Ghosh, B. Norton, T.K. Mallick, Daylight characteristics of a polymer dispersed liquid crystal switchable glazing, Sol. Energy Mater. Sol. Cells 174 (2018) 572—576, https://doi.org/10.1016/j.solmat.2017.09.047.

[31] M. Sudan, G.N. Tiwari, Daylighting and energy performance of a building for composite climate: an experimental study, Alexandria Eng. J. 55 (2016) 3091—3100, https://doi.org/10.1016/j.aej.2016.08.014.

[32] A. Thanachareonkit, J.L. Scartezzini, M. Andersen, Comparing daylighting performance assessment of buildings in scale models and test modules, Sol.

Energy 79 (2005) 168—182, https://doi.org/10.1016/j.solener.2005.01.011.

[33] C.S. McCamy, Correlated color temperature as an explicit function of chromaticity coordinates, Color Res. Appl. 17 (1992) 142—144, https://doi.org/10.1002/col.5080170211.

[34] A. Ghosh, B. Norton, A. Duffy, Measured overall heat transfer coefficient of a suspended particle device switchable glazing, Appl. Energy 159 (2015) 362—369, https://doi.org/10.1016/j.apenergy.2015.09.019.

[35] A. Nabil, J. Mardaljevic, Useful daylight illuminances: a replacement for daylight factors, Energy Build. 38 (2006) 905—913, https://doi.org/10.1016/j.enbuild.2006.03.013.

[36] 75-1988 CIE Publication, Spectral Luminous Efficiency Functions Based upon Brightness Matching for Monochromatic Point Sources with 2° and 10° Fields, 1988, ISBN 3900734119.

[37] C.I. De l'Eclairage, CIE 1988 2 Spectral Luminous Efficiency Function for Photopic Vision, 1990.

[38] Illuminanting Engineering Society of North America, 2015 (n.d).

[39] A. Ghosh, B. Norton, Interior colour rendering of daylight transmitted through a suspended particle device switchable glazing, Sol. Energy Mater. Sol. Cells 163 (2017) 218—223, https://doi.org/10.1016/j.solmat.2017.01.041.

[40] A. Piccolo, A. Pennisi, F. Simone, Daylighting performance of an electrochromic window in a small scale test-cell, Sol. Energy 83 (2009) 832—844, https://doi.org/10.1016/j.solener.2008.11.013.